PHYSICAL REVIEW B VOLUME 62, NUMBER 7 15 AUGUST 2000-I

Pressure dependence of the dielectric and lattice-dynamical properties of GaN and AlN

J.-M. Wagner and F. Bechstedt

Institut für Festkörpertheorie und Theoretische Optik, Friedrich-Schiller-Universität, Max-Wien-Platz 1, D-07743 Jena, Germany

(Received 10 January 2000)

We present *ab initio* calculations of the structural, dielectric, and lattice-dynamical properties of zinc-blende and wurtzite GaN and AlN under hydrostatic pressure, based on a plane-wave pseudopotential method within the density-functional theory. The calculated volume dependence is related to pressure by means of the Vinet equation of state. A linear-response approach to the density-functional theory is used to derive Born effective charges, dielectric constants, and phonon frequencies. The static ionicities, the dynamic charges, and the dielectric constants are found to decrease with pressure, whereas the phonon frequencies show an increasing longitudinal-transverse splitting. The softening behavior of the low-frequency E_2 mode and of the corresponding TA(L) mode is related to strengths of the covalent and ionic forces. Our results are in agreement with recent Raman measurements.

I. INTRODUCTION

Among the III-V semiconductors, the group-III nitrides AlN, GaN, and InN are currently actively investigated in view of their promising potential for short-wavelength electroluminescence devices.[1] Under ambient conditions AlN and GaN crystallize in the hexagonal wurtzite (2H) structure with the space group C_{6v}^4. However, recent epitaxy[2–4] of thin GaN and AlN films has been demonstrated also to result in the cubic zinc-blende (3C) structure with the space group T_d^2.

Different types of epitaxy methods are used to deposit group-III nitride layers.[1–5] Conventional c-plane substrates with a [0001] orientation are Al_2O_3, 6H-SiC, or ZnO. Epilayers are also grown onto an a-plane sapphire substrate, where the (0001) group-III nitride plane is parallel to the $(11\bar{2}0)$ plane of Al_2O_3. In the zinc-blende case [001]-oriented GaAs and 3C-SiC substrates are used. In all these cases the lattice constants of the nitrides and the substrates are quite different. However, although these epitaxies are far from the pseudomorphic growth mode, the strain is not completely relaxed. Moreover, the different thermal expansion coefficients of epilayers and substrate may induce an additional strain during the temperature decrease after deposition.[5] In any case, strain, in particular biaxial strain, plays an important role for the properties of GaN and AlN layers.[6]

The study of the characteristic phonon frequencies is one of the most important keys for the characterization of the strained materials.[7] For a detailed characterization of the strain relief the mode Grüneisen parameter and the phonon deformation potentials have to be known. This knowledge should be supplemented by that of the dependence of the effective ionic charges and the dielectric constants on the actual atomic structure. Hydrostatic pressure studies are helpful to derive these material parameters. Moreover, Raman scattering measurements of zone-center phonon frequencies are now available for wurtzite GaN and AlN as well as for zinc-blende GaN in the presence of hydrostatic pressure.[8–11]

In this paper we present extensive *ab initio* studies of structural, dielectric, and lattice-dynamical properties of GaN and AlN under hydrostatic pressure. Both polytypes, the wurtzite and zinc-blende structure, are considered. In Sec. II we briefly review the underlying computational methods. In the following section, the results obtained are discussed and compared with experimental data. Physical explanations are given for the calculated pressure dependences and the similarities as well as the differences of the properties of the two nitrides. Finally, in Sec. IV, a brief summary is given.

II. COMPUTATIONAL METHOD

The calculations are performed using the plane-wave-pseudopotential approach within the framework of the density-functional theory (DFT). The exchange-correlation energy of the electrons is described in the local-density approximation (LDA) by the Perdew-Zunger interpolation.[12] The valence electron-ion interaction is treated by *ab initio* norm-conserving pseudopotentials.[13] However, there are at least two problems. The common frozen-core approximation breaks down for the Ga3d electrons in GaN due to the energetical resonance of the Ga3d and N2s levels and the overlap of 3d orbitals with the valence electron states. It has been shown[14] that important features of the shallowness of the Ga3d electrons can be treated already within the frozen-core approximation, if the nonlinear core corrections (NLCC) are taken into account according to Louie, Froyen, and Cohen.[15] The second problem arises from the lack of p electrons in the core of the nitrogen atoms. The small N core usually requires a relatively high cutoff energy of the plane-wave expansion of the electron eigenfunctions. For that reason we generate the Ga, Al, and N pseudopotentials according to the scheme of Troullier and Martins.[13] The resulting soft-core potentials allow a restriction of the cutoff energy to values of 75 Ry (2H-GaN and -AlN), 80 Ry (3C-GaN), and 60 Ry (3C-AlN). The summation over the Brillouin zone (BZ) is performed using sets of Chadi-Cohen special points.[16] Convergence of the structural parameters (see below) is reached for 12 (19, 28) special points in the irreducible wedge of the BZ of the wurtzite (zinc-blende AlN, GaN)

 ©2000 The American Physical Society

structures. The values of both parameters, cutoff energy and number of special points, are higher than those used in the previously published phonon data of unstrained group-III nitrides.[14,17,18] The improved accuracy was required to obtain structural results consistent with calculations of the effects of biaxial strain.[19]

The ground-state properties in the pressure-free case are obtained by minimization of the total energy with respect to the unit cell volume V. Whereas in the zinc-blende case the volume is directly related to the lattice constant a_0, for the wurtzite structure this minimization has to be performed by a two-step procedure due to three independent parameters, the lattice constants c and a and the internal cell parameter u that determines the relative bond length between cation and nitrogen atoms parallel to the c axis. For a given unit cell volume $V=\sqrt{3}a^2c/2$ the total energy is minimized with respect to c/a and u. In more detail, for a set of c/a values near equilibrium, first the internal parameter u is determined for each fixed c/a. Then the equilibrium value for c/a is obtained, and finally the equilibrium internal parameter is calculated. These steps are repeated for other volumes near the experimental equilibrium value. The theoretical equilibrium volume V_0, the static bulk modulus at zero pressure, B_0, and first-order pressure derivative of the bulk modulus at zero pressure, B_0', are determined by fitting the total energy as a function of volume to the Vinet equation of state.[20] The finite hydrostatic pressure is simulated by choosing a series of decreasing cell volumes. Since low temperatures are considered, the pressure p is related to the first derivative of the total energy E with respect to the volume by $p=-\partial E/\partial V$.

The lattice-dynamical properties, i.e., eigenfrequencies and eigenvectors of the lattice vibrations, are calculated within the framework of the self-consistent density-functional perturbation theory[21] (DFPT) for a given equilibrium geometry at finite pressure defined by a set of parameters V, c/a, and u. The DFPT also allows the calculation of the high-frequency dielectric tensor, $\boldsymbol{\varepsilon}_\infty$, and the Born effective charge tensor, $\mathbf{Z}_B$, for each inequivalent atom in the unit cell. These quantities are necessary for the nonanalytic part of the dynamical matrix of polar semiconductors like GaN and AlN. The DFPT is generalized to the inclusion of NLCC.[14,17] In the case of the DFPT calculations, convergence is already reached at the kinetic-energy cutoff of 60 Ry (50 Ry) for the wurtzite (zinc-blende) structures. The changes of the phonon frequencies with rising cutoff are typically 2 cm^{-1} or less.

III. RESULTS AND DISCUSSION

A. Structural properties

Results of the total-energy minimizations are represented in Figs. 1 and 2. Using the Vinet equation of state (EOS) the relation between the normalized volume and hydrostatic pressure (at zero temperature) is plotted in Fig. 1, together with some experimental results.[22–24] Only the low-pressure $2H$ and $3C$ structures are considered. The calculated EOS for the two AlN polytypes and the zinc-blende GaN are nearly identical. To obtain the same volume contraction a slightly lower hydrostatic pressure has to be applied in the case of wurtzite GaN, which we find to possess a lower bulk modulus (207 GPa) in comparison to AlN (210 GPa). There is an

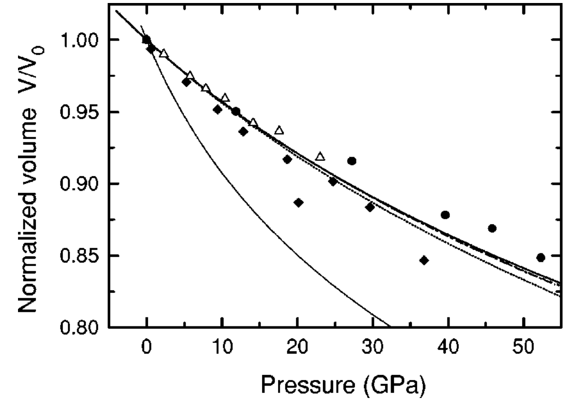

FIG. 1. Normalized volume versus hydrostatic pressure according to the Vinet equation of state for GaN and AlN crystallizing in the two polytype structures $2H$ (wurtzite) and $3C$ (zinc blende). The theoretical cell volume V_0 at zero pressure is used for normalization. For comparison results for zinc-blende GaAs are also given. Solid line: $3C$-GaN; short-dotted line: $2H$-GaN; dashed line: $3C$-AlN; dotted line: $2H$-AlN; thin solid line: GaAs. Experimental results are plotted for $2H$-AlN [open triangles (Ref. 22)] and for $2H$-GaN [filled diamonds (Ref. 23), filled circles (Ref. 24)].

excellent agreement with the experimental data, which show larger deviations among themselves. The low-pressure structures of the nitrides considered here behave very similar with respect to their EOS. Moreover, the difference in the EOS of the nitrides is much smaller than the discrepancy in the volumes for a given pressure when the group-III nitrides are compared with a more common III-V compound, e.g., GaAs. Its stronger variation of the volume with hydrostatic pressure is in agreement with the weaker chemical bonding. The cohesive energy per bond is with 1.63 eV, much smaller than the corresponding values of GaN (2.24 eV) and AlN (2.88 eV).[25]

In contrast to the similarity in the EOS, one knows for GaN and AlN that the wurtzite structure changes over into the cubic rocksalt structure (O_h^5 space group) at remarkably different transition volumes V_t (and hence, pressures). Calculations gave the values of $V_t=0.81V_0$ $(0.94V_0)$ for GaN (AlN), corresponding to a transition pressure of 55.1 GPa (12.9 GPa).[26,27] Experimental results for GaN show a hysteresis (30 GPa for the downstroke and 50 GPa for the upstroke[28]) or give 37 GPa (Ref. 23) and 52.2 GPa (Ref. 24), while for AlN the measured transition pressure is situated between 14 and 16.5 GPa at about 1500 °C (Ref. 29) (at 22.9 GPa for room temperature[22]). This behavior is on the one hand related to the much smaller total-energy difference between NaCl and $2H$ in AlN (Ref. 27) compared with GaN (Ref. 26) (while the corresponding volume changes are comparable). On the other hand, in the case of wurtzite AlN the ratio of the two lattice constants c/a and the internal cell parameter u differ remarkably from the ideal values $\sqrt{8/3}\approx 1.633$ and 0.375 and exhibit a drastic pressure variation away from these values. This indicates that the AlN lattice is more susceptable to distortions already at small hydrostatic pressure values.

The calculated ratio of the two lattice constants c/a and the internal cell parameter u are plotted versus hydrostatic pressure in Figs. 2(a) and 2(b). In GaN the two quantities are rather close to the ideal values. Their pressure dependence is

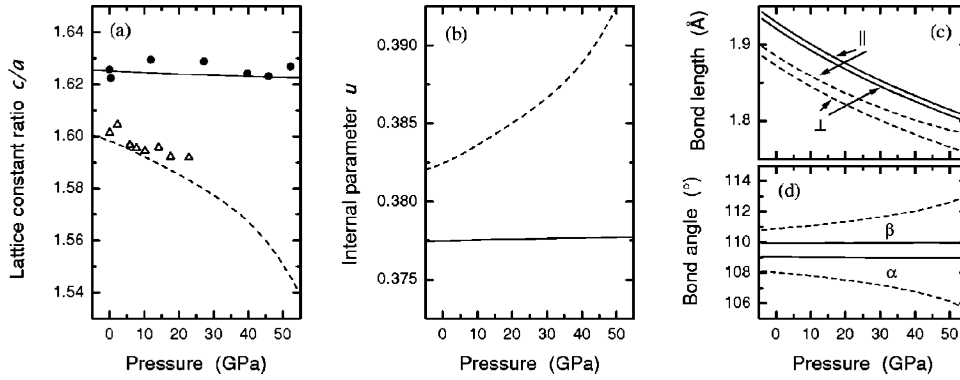

FIG. 2. Structural parameters of wurtzite GaN and AlN under hydrostatic pressure. Solid lines: GaN; dashed lines: AlN. (a) Ratio of the lattice constants c/a versus pressure. Experimental results are plotted for $2H$-AlN [open triangles (Ref. 22)] and for $2H$-GaN [filled circles (Ref. 24)]. (b) Internal parameter u versus pressure. (c) Lengths of the two inequivalent bonds versus pressure. Labeling $\|$: bond along the c axis; $\perp$: bond (nearly) perpendicular to it. (d) Bond angles versus pressure. Labeling α: angle between the c-axis and the bond (nearly) perpendicular to it; β: angle between two bonds (nearly) perpendicular to the c axis.

negligible. We find linear pressure coefficients of $(\partial \frac{c}{a}/\partial p)_{p=0} = -4.7\times 10^{-5}$ and $(\partial u/\partial p)_{p=0} = 5\times 10^{-6}$. In the case of AlN, the situation is completely different. The values c/a (u) are remarkably smaller (larger) than the ideal values and decrease (increase) with rising hydrostatic pressure, with a slope of $(\partial \frac{c}{a}/\partial p)_{p=0} = -5.6\times 10^{-4}$ and $(\partial u/\partial p)_{p=0} = 1.08\times 10^{-4}$. Our results for c/a are in reasonable agreement with experimental studies of the lattice constants under pressure.[22,24] For GaN, a nearly constant c/a was concluded also from optical measurements of the crystal-field splitting under pressure.[30] In previous discussions[18,31,32] the findings for AlN have been traced back to the more pronounced trend to crystallize within the wurtzite structure. The difference $(c/a - \sqrt{8/3})$ is proportional to the energy gain of $2H$ compared to $3C$.[33] It is accompanied by deviations $(u-0.375)$. Assuming nearly equal bond lengths parallel and perpendicular to the c axis [cf. Fig. 2(c)], the relation $u \approx \frac{1}{4} + \frac{1}{3}(a/c)^2$ leads to an internal parameter $u > \frac{3}{8}$, which increases as c/a decreases.

The different pressure behavior of the axial ratio c/a in GaN and AlN can also be expressed by the ratio of the corresponding components of the strain tensor, $\epsilon_{zz}/\epsilon_{xx}$, which we find to amount (in the low-pressure region) to 1.02 for GaN and 1.23 for AlN. This ratio can be expressed by the elastic constants as

$$\frac{\epsilon_{zz}}{\epsilon_{xx}} = \frac{C_{11}+C_{12}-2C_{13}}{C_{33}-C_{13}}. \tag{1}$$

From values for the elastic constants,[34] one finds that for both materials the numerator of Eq. (1) has nearly the same value, whereas the denominator is larger for GaN than that for AlN. The reason for the decreasing value of c/a for AlN is therefore traced back to a different balance between the ''angular'' elastic constant C_{13} and the ''axial'' one C_{33} in comparison with GaN. The latter is much larger in GaN, which is therefore able to sustain the stress in the z direction, $-p = \sigma_{zz} = 2C_{13}\epsilon_{xx} + C_{33}\epsilon_{zz}$, already at smaller absolute strain $|\epsilon_{zz}|$ than in AlN.

As a consequence of the different variations of c/a and u in GaN and AlN, one has different lattice deformations under pressure. In Figs. 2(c) and 2(d) the lengths of the inequivalent bonds and the angles between them are plotted versus hydrostatic pressure. As can be expected from Figs. 2(a) and 2(b), for GaN these quantities are close to those in an ideal tetrahedron (equal bond lengths, identical bond angles of 109.47 °). With rising hydrostatic pressure, indeed the bond angles remain almost constant, i.e., besides the shrinking of the bond lengths there is no remarkable change in the form of the tetrahedral structure. In AlN the significant deviations from the ideal wurtzite structure are further enlarged under pressure. Especially the difference between the bond angles increases in such a way that the zig-zag chains perpendicular to the c axis are flattened, i.e., the bonding tetrahedra are compressed along the c-axis by shrinking the vertical distance $(\frac{1}{2}-u)c$ of the Al-N layers towards a planar structure. This implies a tendency for dehybridization from ideal sp^3 dangling bonds towards sp^2 and p_z orbitals.

The trend to crystallize within the wurtzite structure and, in particular, to have bond angles different from the ideal tetrahedron angles, has often been related to the large ionicity of the chemical bonds. We characterize the bond ionicity by the charge asymmetry coefficient g according to Garcia and Cohen.[35] It is plotted in Fig. 3 versus pressure for the zinc-blende polytypes. We clearly observe a weak decrease of g with rising pressure independent of the nitride (slopes: -3×10^{-4} GPa^{-1} for GaN, -4×10^{-4} GPa^{-1} for AlN).

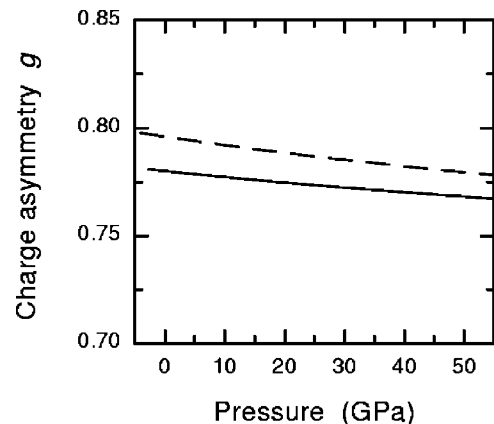

FIG. 3. Charge asymmetry coefficient g versus hydrostatic pressure in the zinc-blende case. Solid line: GaN; dashed line: AlN.

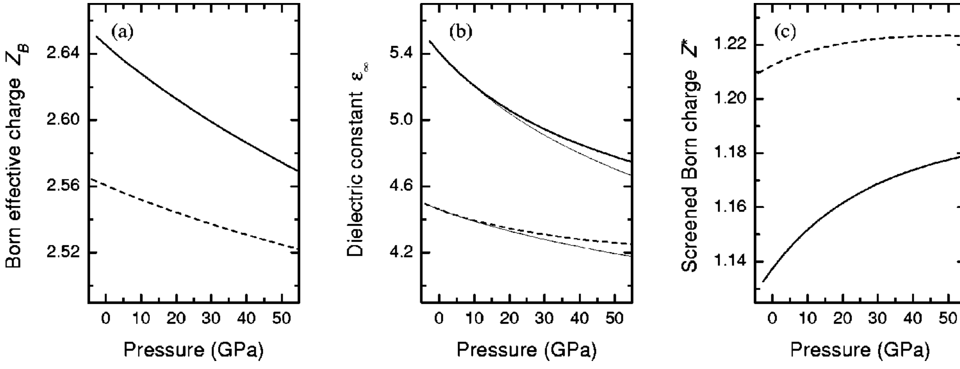

FIG. 4. (a) Born effective charge and (b) high-frequency dielectric constant versus hydrostatic pressure for zinc-blende GaN (solid line) and AlN (dashed line). (c) Resulting screened effective ion charge. Thin lines in (b) represent expression (2).

This finding means that the logarithmic derivative of g with respect to the volume is positive. At least in the AlN case, this behavior is seemingly in contrast to the increase of the deviations of c/a and u from the values of the ideal wurtzite structure, since this is usually related to an increasing bond ionicity. On the other hand, with rising pressure and decreasing bond lengths the overlap of the valence electron wave functions increases. Consequently, the increasing probability to find an electron also closer to the cation results in smaller values of the bond ionicity.

B. Dielectric properties

The long-range macroscopic electric field accompanying several atomic displacements in polar crystals is described by a nonanalytic contribution to the dynamical matrix,[21] consisting of the tensors of the Born effective charges $\mathbf{Z}_B$ and of the high-frequency dielectric constants $\boldsymbol{\varepsilon}_\infty$. They are also calculated in the framework of the DFPT as a first step. In Figs. 4(a) and 4(b), results for the cubic polytypes are presented, where the tensors possess only one independent component. For the wurtzite case the tensor components parallel and perpendicular to the c axis are plotted in Fig. 5. Independent of the polytype and of the nitride the components of the two tensors under consideration decrease monotonically with rising pressure, except for the $(Z_B)_{||}$ component of $2H$-AlN. The latter exhibits a saturation between 10 and 20 GPa, followed by a significant increase. This is likely due to the mentioned dehybridization that accompanies the tetrahedron deformation. In general, the pressure (and hence, volume) dependence is more pronounced for GaN because of the stronger covalent bonding in AlN.

For the Born effective charge, we observe a weak variation with volume as characterized by the logarithmic derivative $(\partial \ln Z_B/\partial \ln V)_{V=V_0}$, which takes the values 0.149 ($3C$-GaN), 0.074 ($3C$-AlN), 0.151 and 0.137 ($||$ and $\perp 2H$-GaN), 0.022 and 0.086 ($||$ and $\perp 2H$-AlN). Previously, a value of 0.139 has been calculated for $3C$-GaN.[36] For not too large pressure values, the decrease is almost linear. The corresponding pressure coefficients $(\partial Z_B/\partial p)_{p=0}$ are -1.8×10^{-3} GPa^{-1} ($3C$-GaN), -9×10^{-4} GPa^{-1} ($3C$-AlN), -2.0×10^{-3} GPa^{-1} and -1.7×10^{-3} GPa^{-1} ($||$ and $\perp 2H$-GaN), -3×10^{-4} GPa^{-1} and -1.0×10^{-3} GPa^{-1} ($||$ and $\perp 2H$-AlN). Using $(\partial \ln\varepsilon_\infty/\partial p)_{p=0} = -3.8\times10^{-3}$ GPa^{-1} and $B_0=200$ GPa an experimental value of $(\partial Z_B/\partial p)_{p=0} = (-2.4\pm0.5)\times10^{-3}$ GPa^{-1} has been derived for the parallel component of $2H$-GaN.[9]

The pressure-induced reduction of the dynamical ion charges indicates a charge redistribution from the nitrogen atoms to the gallium or aluminum atoms in comparison with the pressure-free situation. Although this holds for atoms being displaced from their equilibrium positions, it follows the same trend as already described for the static ionic charge defined by the charge asymmetry coefficient (cf. Fig. 3). The dynamic and the static charges of the cubic polytypes are compared in Fig. 6(a). The charge asymmetry coefficient takes similar values, while the Born effective charge differs for GaN and AlN and, especially, covers different ranges of values. For AlN, which has the higher static ionicity, this range is smaller than that for GaN. Interpreting the static charge asymmetry coefficient g as a bond polarizability, it can be related to the dynamic charge by $Z_B^{\mathrm{model}} = -\frac{1}{2}\Delta Z + 4g + \frac{8}{3}g(1-g^2)$, with $\Delta Z=2$ as the difference between the number of valence electrons of group-III and -V

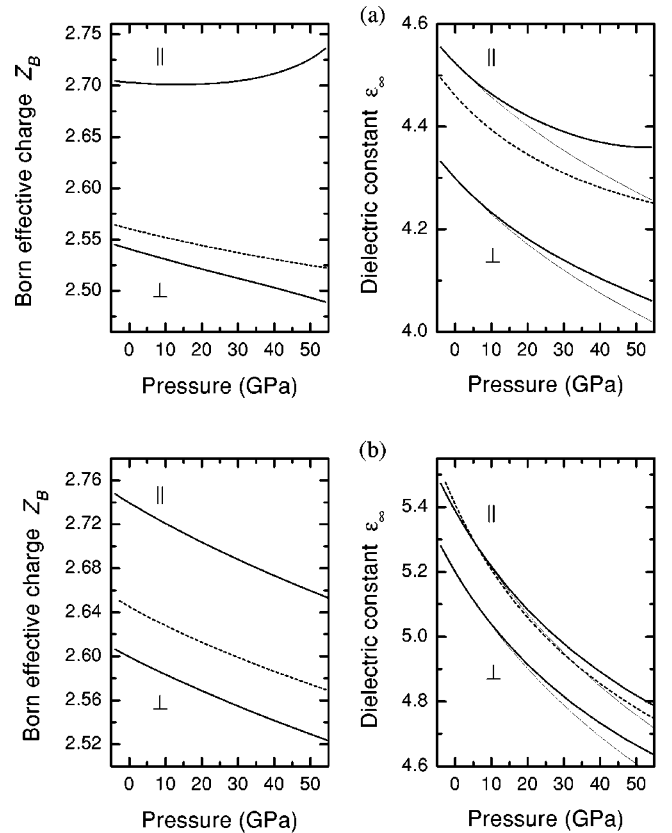

FIG. 5. Pressure dependence of the two independent tensor components of the Born effective charge and the dielectric constant. Upper panels (a): $2H$-AlN; lower panels (b): $2H$-GaN. For comparison the $3C$ results are plotted as dashed lines. Thin lines in the right panels represent expression (2).

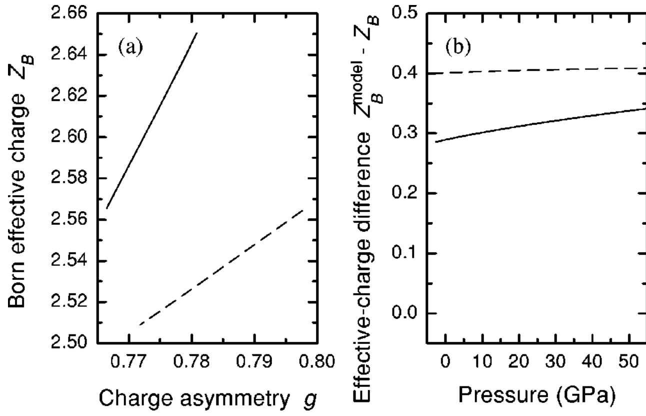

FIG. 6. (a) Comparison of the Born effective charge with the static charge asymmetry coefficient. (b) Difference of the model effective charge (see text) and the *ab initio* result for the Born effective charge versus hydrostatic pressure. Solid line: 3*C*-GaN; dashed line: 3*C*-AlN.

elements.[25] For the nitrides considered here, the g values are rather large, and therefore the use of the model formula leads to an overestimation of the dynamic charge as shown in Fig. 6(b). For AlN, the difference is nearly constant, whereas for GaN it increases with pressure. Therefore, the pressure dependence obtained from the model, $\partial Z_B^{\mathrm{model}}/\partial p=(20/3-8g^2)\partial g/\partial p$, gives correctly that found for AlN, whereas it underestimates that for GaN.

The variation of the high-frequency dielectric constants versus pressure in Figs. 4(b) and 5 (right panels) shows a significant nonlinear behavior already for not too large pressures. According to the bond-orbital model,[25] the underlying volume dependence may be described by

$$\varepsilon_\infty(V)=1+[\varepsilon_\infty(V_0)-1]\frac{\left(\frac{V_0}{V}\right)^{5/3}}{\left\{1+C\left[\left(\frac{V_0}{V}\right)^{4/3}-1\right]\right\}^{3/2}}, \quad (2)$$

with a certain constant C. It is related by

$$C=\frac{1}{2}\left[\frac{B_0}{\varepsilon_\infty(V_0)-1}\left(-\frac{\partial\varepsilon_\infty}{\partial p}\right)_{p=0}+\frac{5}{3}\right]$$

to the bulk modulus B_0 and the linear pressure coefficient. We find the values $C=1.39$ (3*C*-GaN), 1.07 (3*C*-AlN), 1.30 and 1.29 ($\|$ and $\perp$ 2*H*-GaN), as well as 1.05 and 1.08 ($\|$ and $\perp$ 2*H*-AlN). With the relation (2) we obtain an excellent reproduction of the low-pressure range for AlN (below 10 GPa), whereas for GaN the approximation is applicable also to slightly higher pressures (about 15 GPa). This discrepancy again follows the different transition pressures.

Very interesting is the behavior of the screened charges $Z^*=Z_B/\sqrt{\varepsilon_\infty}$ under pressure as presented for the zinc-blende polytypes in Fig. 4(c). There is nearly a compensation of the pressure dependences of the dynamic ionic charge and that of the dielectric constant. As a net effect, the screened charge increases slightly with increasing pressure. For AlN the screened charge varies only in the range $Z^*\approx 1.21-1.22$. Due to the weaker covalent bonds in GaN the net pressure effect on Z^* is more pronounced. There is a tendency for a saturation for rather large pressures. For the hexagonal polytypes one obtains an analogous behavior because of a similar pressure dependence, as can be seen from Fig. 5.

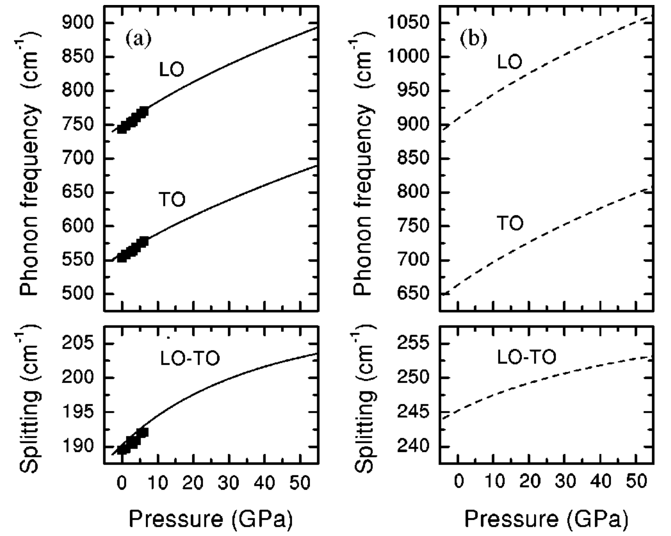

FIG. 7. Pressure dependence of the zone-center optical frequencies for the zinc-blende polytypes (upper panels). The difference of the optical phonon frequencies are plotted in the lower panels. The experimental results (Ref. 10) are indicated by filled squares.

C. Vibrational frequencies

The pressure dependence of the LO and TO Raman frequencies is shown in Fig. 7 for the cubic polytypes 3*C*-GaN (a) and 3*C*-AlN (b). In the lower part their differences are plotted. There is a monotonic increase from the zero-pressure values $\omega_{\mathrm{LO}}(\Gamma)=750$ (907) cm^{-1}, $\omega_{\mathrm{TO}}(\Gamma)=560$ (662) cm^{-1}, and $\omega_{\mathrm{LO}}(\Gamma)-\omega_{\mathrm{TO}}(\Gamma)=190$ (245) cm^{-1} for GaN (AlN) (Refs. 17 and 18) with rising hydrostatic pressure. In the low-pressure region the calculations essentially reproduce the Raman measurements for 3*C*-GaN.[10,37] The physics of this behavior can be explained using a description with elastic bond-stretching and bond-bending forces within a Keating model[38] and, respectively, of the Coulomb forces by an Ewald summation technique.[39] The two characteristic zone-center frequencies follow within this model as[40]

$$\omega_{\mathrm{LO/TO}}^2(\Gamma)=\left(\frac{1}{M_c}+\frac{1}{M_N}\right)(4\alpha+4\beta+c_{\mathrm{LO/TO}}\hat{f}) \quad (3)$$

with the cation mass M_c, the nitrogen mass M_N, the radial (α) and angular (β) force constant of the Keating model, $c_{\mathrm{LO}}=2/3$, $c_{\mathrm{TO}}=-1/3$, and the Coulomb force constant

$$\hat{f}=\frac{e^2Z_B^2}{\varepsilon_0\varepsilon_\infty V}, \quad (4)$$

with the vacuum dielectric constant ε_0 and the volume of the primitive cell V. The increase of $\omega_{\mathrm{LO}}(\Gamma)$ and $\omega_{\mathrm{TO}}(\Gamma)$ mainly follows the increase of the radial force constant $\alpha\sim 1/d^n$ with decreasing bond length d but is modified by the increase of the Coulomb force constant. The increase of the LO-TO splittings of GaN and AlN in Fig. 7 is in contrast to the behavior of most of the other III-V semiconductors including

TABLE I. Mode Grüneisen parameter γ_j for cubic GaN and AlN. Other calculated and experimental values are also given. Besides values for zone-center modes also those of phonons at the zone boundary (L point) are listed for comparison with zone-center wurtzite modes.

	Reference	LO(Γ)	TO(Γ)	LO(Γ)-TO(Γ)	LO(L)	TO(L)	LA(L)	TA(L)
GaN	This work	1.02	1.19	0.5	1.05	1.23	0.92	−0.49
	Calc. 42		1.8					
	Calc. 43		1.52					
	Expt. 10	1.20	1.4	0.5				
AlN	This work	0.89	1.14	0.2	0.96	1.31	0.85	−0.29
	Calc. 42		1.5					
	Calc. 43		1.42					

BN.[41] The reason is the net pressure effect discussed above for the screened ion charge. The effect of the increase of $Z_B/\sqrt{\varepsilon_\infty}$ is enhanced by the effect of the $1/V$ factor in the Coulomb force constant in Eq. (4). Therefore, although the LO-TO splitting of GaN and AlN increases, these materials become less ionic with pressure, in contrast to SiC.[31]

The low-pressure behavior is dominated by the mode Grüneisen parameter

$$\gamma_j = -\left.\frac{\partial \ln\omega_j}{\partial \ln V}\right|_{V=V_0} = B_0 \left.\frac{\partial \ln\omega_j}{\partial p}\right|_{p=0} \tag{5}$$

for a phonon mode j with the frequency ω_j. Calculated and measured values are collected in Table I for the cubic crystals. The present calculation as well as the available linear-muffin-tin-orbital (LMTO) studies of the TO phonon[42,43] give larger Grüneisen parameters for GaN in comparison with AlN as a consequence of the stronger covalent bonding in AlN and, therefore, larger force constants $\alpha+\beta$. Thereby, our plane-wave results underestimate the experimental GaN values, whereas the LMTO treatments give too large a mode Grüneisen parameter γ_{TO}. We mention that within the DFPT approach the long-range electric field is correctly treated including its nonanalytic behavior in the noncubic case. The large experimental values may be related to the quality of the extremely thin cubic GaN layers, which makes a homogeneously strained material unlikely. Another source for the discrepancy is the use of different bulk moduli B_0 in the determination of the Grüneisen parameters.

The pressure dependence of all zone-center modes in the wurtzite crystals is plotted in Fig. 8 (2H-GaN) and Fig. 9 (2H-AlN). More in detail, the Raman-active modes E_1(LO), A_1(LO), upper E_2 (twofold degenerate), E_1(TO), A_1(TO), and lower E_2 (twofold degenerate) are shown together with the two silent B_1 modes. The Raman frequencies at zero pressure are 757 (924), 748 (898), 576 (667), 568 (677), 540 (618), 142 (241) cm^{-1} for 2H-GaN (2H-AlN). Generally, with the exception of the lower E_2 modes, the phonon frequencies increase with rising pressure for reasons that have already been discussed in the zinc-blende case. The agreement with the pressure dependences found experimentally is reasonable. It is remarkably improved considering the LO-TO splittings in the lower panels of Figs. 8 and 9. With the exception of those of the lower E_2 modes, the mode Grüneisen parameters in Table II are positive. They are rather close to the value discussed in the zinc-blende case. This also holds for the fact that the GaN values are larger, except for the upper E_2 mode, where the Grüneisen parameter is slightly larger for AlN. One set of experimental values for 2H-AlN (Ref. 44) seems to fall off the common trend and should be used with care, especially since the authors do not confirm these results in a subsequent work.[45] The anomalous behavior of the lower E_2 modes will be discussed below.

Over the whole pressure range plotted in Figs. 8 and 9, there is a remarkable difference between 2H-GaN and 2H-AlN concerning the A_1 and the B_1 modes. They show a significant drop in their pressure sensitivity for AlN, or even a saturationlike behavior. The excitation of these modes is accompanied by atomic displacements along the c axis. Consequently, the high-pressure behavior is related to the structural changes as discussed for the internal parameter u. In

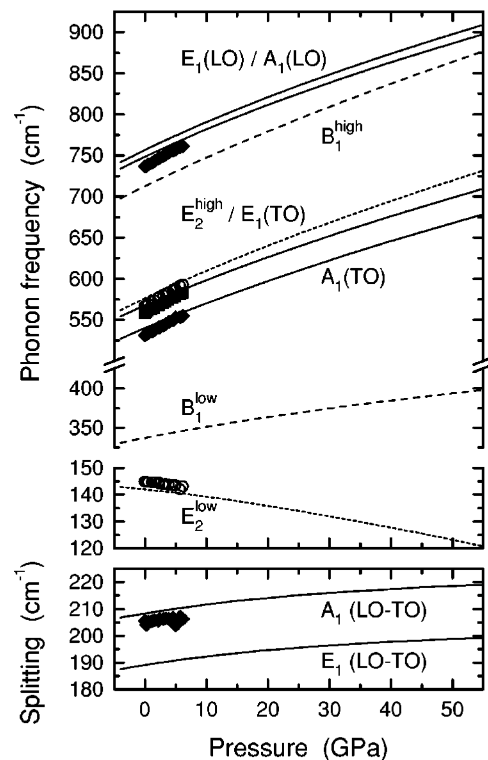

FIG. 8. Pressure dependence of the zone-center optical frequencies for the wurtzite GaN (upper panel). Difference frequencies of LO and TO phonons of the same symmetry (lower panel). Experimental results (Ref. 10) are included (filled diamonds, A_1 modes; open circles, E_2 modes; filled squares, E_1 mode).

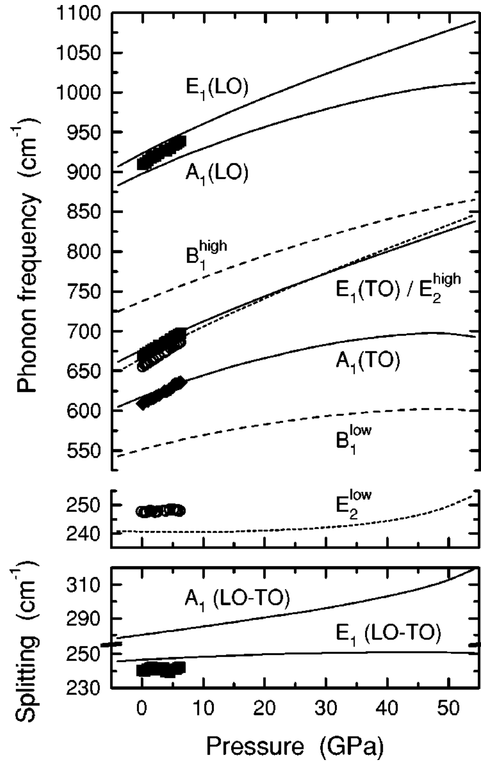

FIG. 9. Pressure dependence of the zone-center optical frequencies for the wurtzite AlN (upper panel). Difference frequencies of LO and TO phonons of the same symmetry (lower panel). Experimental results (Ref. 11) are included (filled squares, E_1 modes; open circles, E_2 modes; filled diamonds, A_1 mode).

fact, a phonon calculation with an unchanged smaller value of u that keeps the AlN lattice closer to the ideal tetrahedral geometry results in an increase of the A_1 and B_1 frequencies and a lowering of the E_1 and the E_2 mode frequencies.[19] As a precursor of the saturation, the different pressure dependence of the A_1-E_1 pair of the LO and the TO modes is noticeable already at low pressures, indicating the increasing anisotropy of 2H-AlN with rising pressure.

Similar to the cubic crystals, the ionicity of the wurtzite structure reveals itself in the splitting of the LO and TO modes. Because of the uniaxial crystal symmetry, for a quantitative evaluation one has to take into account the different mode symmetries. It holds for the corresponding displacement directions[46] ($\alpha = x,z$) that

$$\omega_{\mathrm{LO}}^2(\alpha) - \omega_{\mathrm{TO}}^2(\alpha) = \frac{2e^2(Z_B)_{\alpha\alpha}^2}{\varepsilon_0(\varepsilon_\infty)_{\alpha\alpha} V\mu}, \tag{6}$$

with the reduced mass μ of an anion-cation pair. The increasing LO-TO splitting, which is observed theoretically and experimentally for both nitrides (cf. the lower panels of Figs. 8 and 9), is therefore due to the pressure behavior of the corresponding components of the dynamic effective charge tensor and of the dielectric constant, respectively, where the (parallel) z components apply to the modes with A_1 symmetry and the (perpendicular) x components to those with E_1 symmetry. By comparison with the results for the cubic case in Fig. 5, one derives the same interpretation for the wurtzite case. The screening of the decreasing dynamic charge is reduced, and the increasing LO-TO splitting is not due to an increase in ionicity. Our results are in contrast to the experiments of Perlin *et al.*,[9] who found a decreasing splitting of the A_1 modes in 2H-GaN. However, their LO and TO modes were measured independently from two different samples, whereas the experimental results cited here were obtained from the same sample.[10]

For the lower E_2 modes of 2H-GaN and 2H-AlN we find Grüneisen parameters that are negative or nearly zero in reliable agreement with the Raman measurements.[10,11,44,45] Consequently the E_2^{low} modes soften in the presence of hydrostatic pressure. At least two questions arise: (i) Why does such a softening occur for the E_2 modes? (ii) Why is the softening in AlN much weaker than that in GaN?

According to the folding relationship between points in the zinc-blende and wurtzite Brillouin zones, the lowest E_2 modes at Γ in wurtzite correspond to TA(L) modes of the zinc-blende structure. This is confirmed by the fact that the Grüneisen parameter of the TA(L) modes $\gamma_{\mathrm{TA}(L)} = -0.5$ and -0.3 for 3C-GaN and 3C-AlN, respectively, have the same sign and ordering as those of the corresponding E_2 modes of the wurtzite structures. In general, the softening of TA modes at the zone boundary under hydrostatic pressure is observed in several crystals,[47] and hence the softening of the E_2^{low} modes is not surprising. The sign and the ordering of $\gamma_{\mathrm{TA}(L)}$ basically follow the explanation given for the pure covalent material Si and diamond in terms of the interplay of bond-bending and bond-stretching forces.[48] However, there are modifications for GaN and AlN due to the ionic bonding and the quite different atomic masses. Within the simple

TABLE II. Mode Grüneisen parameter γ_j for the zone-center phonons in hexagonal GaN and AlN. Other calculated and experimental values are given for comparison.

	Reference	E_1(LO)	A_1(LO)	E_2 (high)	E_1(TO)	A_1(TO)	E_2 (low)
GaN	This work	0.99	0.98	1.28	1.19	1.21	−0.35
	Calc. 43			1.60	1.48	1.52	−0.20
	Expt. 10		1.20	1.50	1.41	1.51	−0.4
	Expt. 44			1.80	1.61	1.18	−0.43
AlN	This work	0.91	0.82	1.34	1.18	1.02	−0.02
	Calc. 43			1.66	1.48	1.50	−0.28
	Expt. 11	1.06		1.58	1.41	1.51	0.1
	Expt. 41	1.0	1.0		1.6	1.6	
	Expt. 45	0.38; 0.4		1.26; 1.34		1.58; 1.68	≈0
	Expt. 44	1.65		2.38		1.48	≈0

model for the elastic and electrostatic forces between displaced atoms, which we have discussed above, one has in the limit $M_N \ll M_c$ and dominating radial force constants[40]

$$\omega^2_{\mathrm{TA}(L)} \approx \frac{1}{M_c}(4\alpha - c\hat{f})\frac{\hat{S}}{8\alpha} \tag{7}$$

with a constant $c<1$. Consequently, we expect that the pressure dependence of the lower E_2 mode is in addition influence by a sensitive balance of elastic forces and the Coulomb forces, which enter expression (7) with opposite signs. This may explain why the compensation of contributions of the different force contributions is more complete in AlN compared to GaN with the result $|\gamma^{\mathrm{AlN}}_{E_2(\mathrm{low})}| < |\gamma^{\mathrm{GaN}}_{E_2(\mathrm{low})}|$.

IV. SUMMARY

In summary, we have presented *ab initio* calculations in the framework of the DFPT for the pressure dependence of structural, dielectric, and, in particular, lattice-dynamical properties of the group-III nitrides, GaN and AlN, in cubic (zinc-blende) as well as hexagonal (wurtzite) crystal modification. The results for the lattice constants, Born effective charges, dielectric constants, and phonon frequencies agree well with experimental data and other DFT LDA calculations. The equation of state and the pressure dependence of the wurtzite parameters c/a and u, as measured by high-pressure x-ray diffraction studies, can be widely explained. A detailed analysis of the volume and pressure dependences of the Born effective charges and the high-frequency electronic dielectric constants leads to the understanding why the LO-TO splitting in the nitrides increases with rising pressure in contrast to the common III-V compounds. The complicated interplay of the pressure dependences of different contributing quantities, effective charge, dielectric constant, and volume, has to be considered.

The pressure dependences of all vibrational modes related to optical phonon branches are rather similar and independent of the polytype of the nitride. The mode Grüneisen parameters are positive and of the same magnitude. Small deviations between GaN and AlN can be traced back to the stronger covalent bonding in AlN. In agreement with Raman measurements, we observe negative but differing Grüneisen parameters for the lower E_2 modes in the wurtzite structures. We give an explanation using the relation between the lower E_2 mode in $2H$ and the TA(L) phonons in $3C$ by folding arguments. The weakness of the effect in AlN compared to GaN is found as a result of the stronger elastic forces in AlN due to the stronger covalent bonds and of the weaker increase of the Coulomb force constant.

ACKNOWLEDGMENTS

We wish to thank K. Karch for providing preliminary results. This work has been supported by the Deutsche Forschungsgemeinschaft under Contract No. Be 1346/8-4. A considerable part of the computations has been performed on the Cray T90 of the NIC in the Forschungszentrum Jülich.

[1] S. Nakamura, *The Blue Laser Diode—GaN Based Light Emitters and Lasers* (Springer, Berlin, 1997).

[2] O. Brandt, H. Yang, B. Jenichen, Y. Suzuki, L. Däweritz, and K. Ploog, Phys. Rev. B **52**, R2253 (1995).

[3] D. Schikora, M. Hankeln, D. J. As, K. Lischka, T. Litz, A. Waag, T. Buhrow, and F. Henneberger, Phys. Rev. B **54**, R8381 (1996).

[4] H. Okumura, H. Hamaguchi, T. Koizumui, K. Balanishi, T. Nagatomo, and S. Yoshida, J. Cryst. Growth **189/190**, 390 (1998).

[5] C. Kisielowski, J. Krüger, S. Ruvimov, T. Suski, J. W. Ager III, E. Jones, Z. Liliental-Weber, M. Rubin, E. R. Weber, M. D. Bremser, and R. F. Davis, Phys. Rev. B **54**, 17 745 (1996).

[6] W. G. Perry, T. Zheleva, M. D. Bremser, and R. F. Davis, J. Electron. Mater. **26**, 224 (1997).

[7] F. Demangeot, J. Frandon, M. A. Renucci, O. Briot, B. Gil, and R.-L. Aulombard, MRS Internet J. Nitride Semicond. Res. **1**, 23 (1996).

[8] P. Perlin, C. Jauberthie-Carillon, J. P. Itie, A. San Miguel, I. Grzegory, and A. Polian, Phys. Rev. B **45**, 83 (1992).

[9] P. Perlin, T. Suski, J. W. Ager III, G. Conti, A. Polian, N. E. Christensen, I. Gorczyca, I. Grzegory, E. R. Weber, and E. E. Haller, Phys. Rev. B **60**, 1480 (1999).

[10] H. Siegle, A. R. Goñi, C. Thomsen, C. Ulrich, K. Syassen, B. Schöttker, D. J. As, and D. Schikora, in *Gallium Nitride and Related Materials II*, edited by C. R. Abernathy, H. Amano, and J. C. Zolper, MRS Symposia Proceedings No. 468 (Materials Research Society, Pittsburgh, 1997), p. 225.

[11] H. Siegle, J.-M. Wagner, A. R. Goñi, F. Bechstedt, C. Thomsen, and K. Syassen (unpublished); H. Siegle, Ph.D. thesis, Wissenschaft und Technik Verlag, Berlin, 1998.

[12] P. Perdew and A. Zunger, Phys. Rev. B **23**, 5048 (1981).

[13] N. Troullier and J. L. Martins, Phys. Rev. B **43**, 1993 (1991).

[14] K. Karch, F. Bechstedt, and T. Pletl, Phys. Rev. B **56**, 3560 (1997).

[15] S. G. Louie, S. Froyen, and M. L. Cohen, Phys. Rev. B **26**, 1738 (1982).

[16] D. J. Chadi and M. L. Cohen, Phys. Rev. B **8**, 5747 (1973).

[17] K. Karch, J.-M. Wagner, and F. Bechstedt, Phys. Rev. B **57**, 7043 (1998).

[18] K. Karch and F. Bechstedt, Phys. Rev. B **56**, 7404 (1997).

[19] J.-M. Wagner and F. Bechstedt, Phys. Status Solidi B **216**, 793 (1999).

[20] P. Vinet, J. Ferrante, J. R. Smith, and J. H. Rose, J. Phys. C **19**, L467 (1986).

[21] P. Giannozzi, S. De Gironcoli, P. Pavone, and S. Baroni, Phys. Rev. B **43**, 7231 (1991).

[22] M. Ueno, A. Onodera, O. Shimomura, and K. Takemura, Phys. Rev. B **45**, 10 123 (1992).

[23] H. Xia, Q. Xia, and A. L. Ruoff, Phys. Rev. B **47**, 12 925 (1993).

[24] M. Ueno, M. Yoshida, A. Onodera, O. Shimomura, and K. Takemura, Phys. Rev. B **49**, 14 (1994).

[25] W. A. Harrison, *Electronic Structure and the Properties of Solids* (Dover, New York, 1989).

[26] P. E. Van Camp, V. E. Van Doren, and J. T. Devreese, Solid State Commun. **81**, 23 (1992).

[27] P. E. Van Camp, V. E. Van Doren, and J. T. Devreese, Phys. Rev. B **44**, 9056 (1991).

[28] P. Perlin, C. Jauberthie-Carillon, J. P. Itie, A. San Miguel, I. Grzegory, and A. Polian, High Press. Res. **7**, 96 (1991).
[29] H. Vollstädt, E. Ito, M. Akaishi, S. Akimoto, and O. Fukunaga, Proc. Jpn. Acad., Ser. B: Phys. Biol. Sci. **66**, 7 (1990).
[30] Z. X. Liu, K. P. Korona, K. Syassen, J. Kuhl, K. Pakuła, J. M. Baranowski, I. Grzegory, and S. Porowski, Solid State Commun. **108**, 433 (1998).
[31] K. Karch, F. Bechstedt, P. Pavone, and D. Strauch, Phys. Rev. B **53**, 13 400 (1996).
[32] C.-Y. Yeh, Z. W. Lu, S. Froyen, and A. Zunger, Phys. Rev. B **46**, 10 086 (1992).
[33] P. Lawaetz, Phys. Rev. B **5**, 4039 (1972).
[34] A. F. Wright, J. Appl. Phys. **82**, 2833 (1997).
[35] A. Garcia and M. L. Cohen, Phys. Rev. B **47**, 4215 (1993).
[36] T. Sengstag, N. Binggeli, and A. Baldereschi, Phys. Rev. B **52**, R8613 (1995).
[37] K. Karch, J.-M. Wagner, H. Siegle, C. Thomsen, and F. Bechstedt, in *Proceedings of the 7th International Conference on SiC, III-Nitrides and Related Materials*, edited by G. Pensl, H. Morkoç, B. Monemar, and E. Janzén (Trans Tech, Zürich, 1998), p. 303.
[38] P. N. Keating, Phys. Rev. **145**, 627 (1966).
[39] G. P. Srivastava, *The Physics of Phonons* (Hilger, London, 1990).
[40] H. Grille, Ch. Schnittler, and F. Bechstedt, Phys. Rev. B **61**, 6091 (2000).
[41] J. A. Sanjurjo, E. López-Cruz, P. Vogl, and M. Cardona, Phys. Rev. B **28**, 4579 (1983).
[42] K. Kim, W. R. L. Lambrecht, and B. Segall, Phys. Rev. B **53**, 16 310 (1996).
[43] I. Gorczyca, N. E. Christensen, E. L. Peltzer y Blanca, and C. O. Rodiguez, Phys. Rev. B **51**, 11 936 (1995).
[44] P. Perlin, A. Polian, J. P. Itie, I. Grzegory, E. Litwin-Staszewska, and T. Suski, Physica B **185**, 426 (1993).
[45] P. Perlin, A. Polian, and T. Suski, Phys. Rev. B **47**, 2874 (1993).
[46] G. Venkataraman, L. A. Feldkamp, and V. C. Sahni, *Dynamics of Perfect Crystals* (MIT Press, Cambridge, Massachusetts, 1975).
[47] B. A. Weinstein and R. Zallen, in *Light Scattering in Solids IV*, edited by M. Cardona and G. Güntherodt, Topics in Applied Physics No. 54 (Springer, Berlin, Heidelberg, 1984), p. 463ff.
[48] C. H. Xu, C. Z. Wang, C. T. Chan, and K. M. Ho, Phys. Rev. B **43**, 5024 (1991).